

Fully Polymeric Solar Panels: a Real-Time Study of Active-Layer Structure Formation

D. V. Anokhin^{a, b}, K. L. Gerasimov^a, S. Grigoryan^c, D. R. Strel'tsov^{d, e}, A. Kirii^f, and D. A. Ivanov^{a, g*}

^a Faculty of Fundamental Physical-Chemical Engineering, Moscow State University, Moscow, 119991 Russia

^b Institute of Problems of Chemical Physics, Russian Academy of Sciences, Chernogolovka, Moscow oblast, 142432 Russia

^c Solid State Physics, University of Siegen, Siegen, D-57068 Germany

^d Enikolopov Institute of Synthetic Polymeric Materials, Russian Academy of Sciences, Moscow, 117393 Russia

^e National Research Center “Kurchatov Institute”, Moscow, 123182 Russia

^f Leibniz Institute of Polymer Research Dresden, Dresden, D-01069 Germany

^g Institut de Sciences des Matériaux de Mulhouse - IS2M, CNRS UMR7361, Mulhouse, 68057 France

*e-mail: dimitri.ivanov@uha.fr

Received December 28, 2015; in final form, August 10, 2016

Abstract—The effect of solvent and thermal annealing on the structure of active layers in polymer–polymer solar panels has been studied. It has been established by atomic force microscopy (AFM) and X-ray grazing-incidence diffraction that the annealing of films improves phase separation and produces domains that are more compact. Real-time studies have also been carried out on the formation of films of nonpolar (toluene) and polar (chlorobenzene) solvents with simultaneous measurement of the structure and conductivity of the films. It has been established that in both cases the formation of the structures of donor and acceptor domains is a two-stage process, with the stages, however, being noticeably different and determined by physical and chemical properties of the solvents.

DOI: 10.1134/S1995078016060021

INTRODUCTION

Organic solar panels present the result of advancement of a technology that uses organic semiconductors as the material for an active layer that transforms sunlight energy into electricity [1–3]. Although the efficiency of silicon-based devices is still well in excess of that for organic solar panels, organic materials with conjugate systems of bonds possess very high absorption coefficients as compared to silicon. This makes it possible to manufacture devices with active-layer thicknesses of less than one micrometer. Such organic materials can be applied to flexible substrates using roll-up technologies at ordinary temperatures; this allows one to achieve a very high productivity of manufacturing lines for organic solar panels. As a result of considerable cost savings in manufacturing, the expenditures are mainly determined by the costs of organic semiconducting materials themselves, which are consumed at a rate of 1 g per 1 m². For these reasons, organic solar elements have a great potential for fabricating inexpensive large-area sources of renewable energy within the concept of so-called “green energy.” In addition, organic solar elements are flexible; this opens up new doors for their practical application.

Polymer–polymer solar elements, in which semi-conducting polymers play the role of both donors and acceptors of electrons, are an alternative to the classical fullerene-based solar panels, as they have higher light-absorption efficiency. In addition, the donor and acceptor energy levels in this case are easier to optimize, with the production being more technologically effective and ecologically clean [4–7].

The main obstacle in the way of implementing polymer–polymer solar panels is currently their low efficiency. This is explained by the nonoptimal morphology of the active layer, especially of the donor–acceptor interface; this is the reason for the high degree of geminate or nongeminate recombination. Controlling the morphology of polymer–polymer solar panels is one of the ways to improve their performance. The advances in this area are related to developing new electron–acceptor polymers that demonstrate high electron mobility in the initial state and in a mixture; combined with optimum electron affinity, this makes these polymers highly compatible with the newest donor–polymers. A donor–acceptor copolymer based on poly [2,3-bis (3-oktyloxyphenyl) quinoxaline-5,8-diyl-alt-thiophene-2,5-diyl] (PTQ) as a donor and poly ([N,N'-bis(2-oktyldodecyl)-naphthalene-1,4,5,8-bis(dicarboxylamide)-2,6-diyl]-alt-

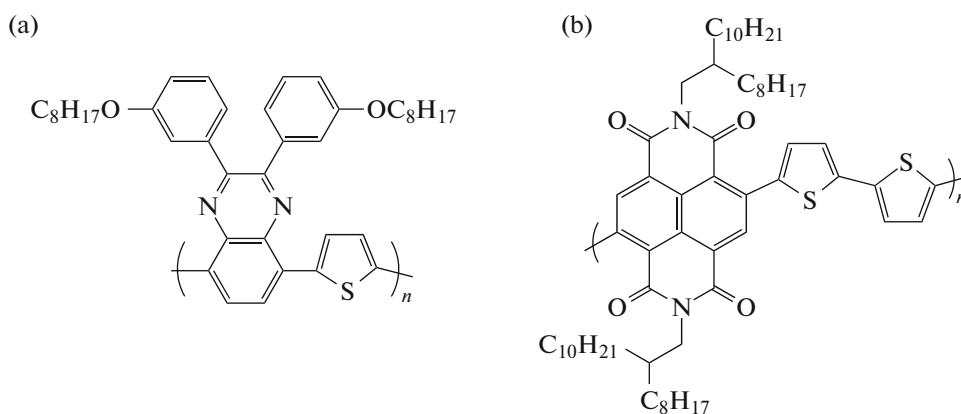


Fig. 1. Chemical structures of (a) PTQ and (b) PNDIT.

5,5'-(2,2'-bithiophene)) (PNDIT) as an acceptor is a prototype of such high-productivity polymers (Fig. 1). PNDIT polymer has exceptionally high electron mobility. In addition, the great electron affinity (~ 4 eV), the narrow width of optically forbidden zone (~ 1.45 eV), and an effective combination of optoelectronic properties makes PNDIT polymer a good candidate for the role of electron-acceptor polymer in polymer–polymer solar batteries [8–12].

It is known from the polymer material science that the process in which the morphology of polymer mixtures is formed is rather complicated and may include several stages that are affected by a variety of factors. For example, the mixture composition, as well as conditions under which it was prepared, including the annealing temperature, are important for the formation of the bulk heterostructure [13]. The efficiency of the spatial heterojunction in polymer–polymer solar cells can be optimized by controlling the morphology of donor–acceptor interfaces immediately during the formation of the active layer. We have shown previously [14–16] that the structural analysis of a film of organic semiconductors during its formation with a specially designed measurement cell is highly effective. An articulate interconnection between the structure evolution and changes in the film conductivity was demonstrated. In the current work, we will use the same approach for a real-time study of the formation of a mixture of donor (PTQ) and acceptor (PNDIT), depending on the solvent used. The film structure is characterized by grazing-incidence wide-angle X-ray scattering (GIWAXS) accompanied by measurements of the film conductivity, as well as by atomic force microscopy (AFM).

EXPERIMENTAL PART

Film Preparation

Films were prepared in a chloroform solution of the equimolar mixture of donor (PTQ1) and acceptor (PNDIT2) with a concentration of 10 mg/mL. The

solvent was heated to a temperature of 75°C . Then, a premanufactured sample of polymers was gradually added to the solvent and the solution of required components in the optimum ratio was obtained with a magnetic agitator [17]. The solution was spin coated onto silicon substrates with dimensions of 20×20 mm with a rate of rotation of 2000 rpm. The obtained films were annealed on a Linkam warm stage at a temperature of 100°C for 10 min.

For X-ray structure analysis, the solutions of the equimolar mixture of donor (PTQ1) and acceptor (PNDIT2) with a concentration of 10 mg/mL were prepared in chlorobenzene and toluene. The solution was mixed with a magnetic agitator at a temperature of 50°C for 30 min to complete the dissolution of the components.

Atomic Force Microscopy

The morphology of the film surface before and after annealing was studied by AFM. Measurements were taken with a Bruker Multimode 8 microscope equipped with a Nanoscope V controller in the Peak-Force Tapping mode. Bruker SNL-10A probes with a force constant of 0.35 N/m and a resonance frequency of 65 kHz were used. All measurements were taken in air at room temperature.

X-Ray Structure Analysis

Experiments on grazing-incidence wide-angle X-ray scattering were conducted on the BM26 line at the European Synchrotron Radiation Facility (Grenoble, France). Diffraction patterns were registered with a Pilatus 300k detector (the pixel size of 172×172 μm pixels). The wavelength was 1.24 \AA . Measurements were taken on thin films on silicon substrates with an angle of incidence of 0.16° . The magnitude of the scattering vector was calibrated with several diffraction orders from silver behenate. Glass substrates with a size of 18×18 mm were cleansed in an ultrasonic bath

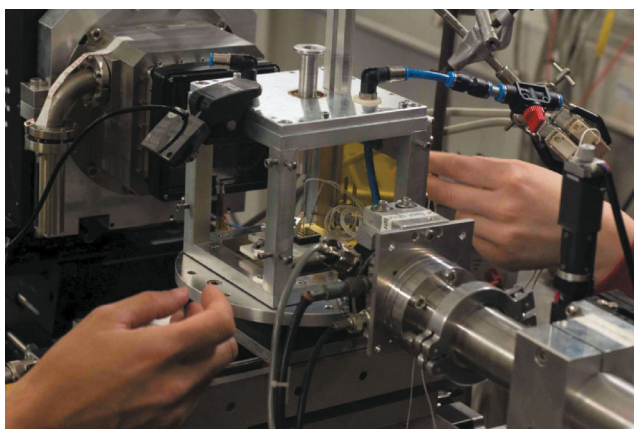


Fig. 2. (Color online) Exterior view of the film-conductivity measurement cell.

filled with Hellmanex II solution and then in 2-propanol and acetone for 20 min. After this, the substrates were rinsed with distilled water. For in situ experi-

ments, electrodes were applied to the substrate by evaporation of gold onto a mask with channels that had a length of 0.1, 1, and 2 mm and a width of 2 mm. The conductivity was measured with a specially designed cell (Fig. 2). The direct voltage of 10 V was applied across the golden electrodes with a Keithley 2400 SourceMeter facility that was controlled within the LabView environment. The intensities of diffraction peaks were analyzed with an in-house piece of software that was created within the Igor Pro environment (Wavemetrics Ltd.).

RESULTS AND DISCUSSION

Figure 3 presents topographic images of the surface of thin films of active layers of solar panels that were obtained by AFM before and after annealing. It can be seen that the samples have a fine-grained domain structure (see Fig. 3). A pair correlation function was constructed from the AFM data for quantitative analysis of the surface roughness. The lateral correlation

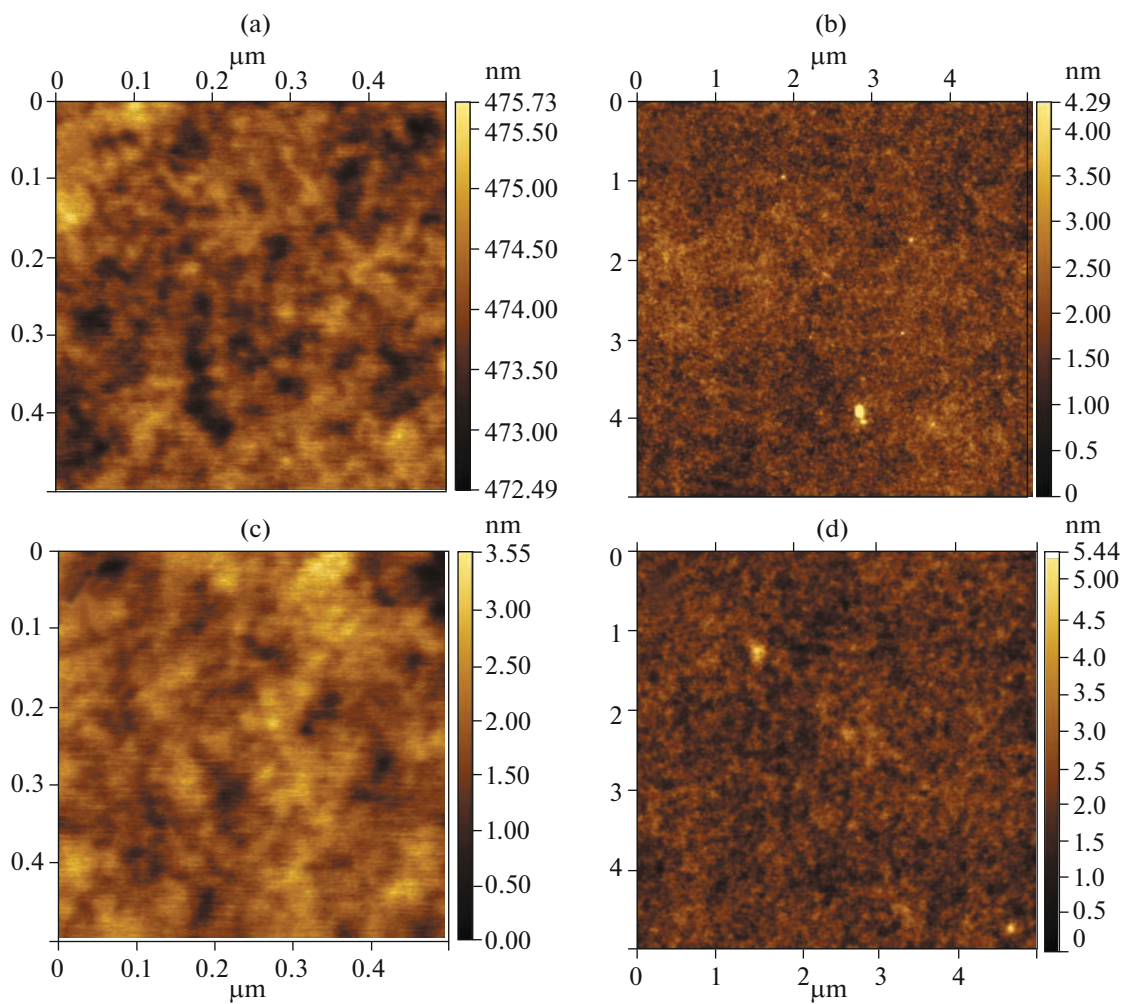


Fig. 3. (Color online) AFM images of the topography of the surface of thin films of donor (PTQ1), which is a component in the active layers of solar panels (a, b) prior to and (c, d) and after annealing on two different scales: (a, c) $0.5 \times 0.5 \mu\text{m}^2$ and (b, d) $5 \times 5 \mu\text{m}^2$.

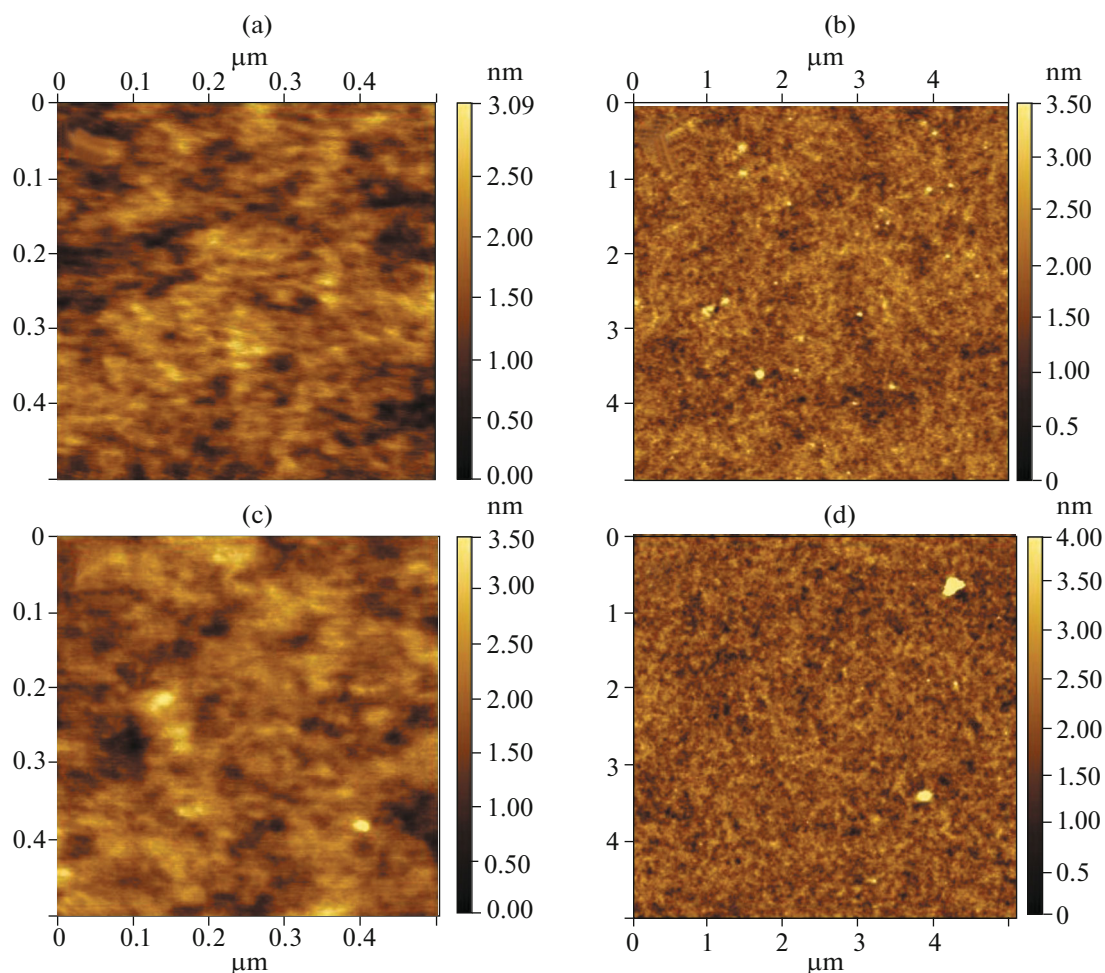


Fig. 4. (Color online) AFM images of the topography of the surface of thin films of a mixture of donor (PTQ) and acceptor (PNDIT) in the active layers of solar panels (a, b) prior to and (c, d) after annealing on two different scales: (a, c) $0.5 \times 0.5 \mu\text{m}^2$, (b, d) $5 \times 5 \mu\text{m}^2$.

and root-mean-square surface roughness were determined from the pair correlation function. The procedure of surface roughness analysis is described in greater detail in [18]. For films of the original donor, thermal annealing increases the lateral correlation length and root-mean-square roughness from 43 and 0.4 to 50 and 0.5 nm, respectively. The calculation is performed for an AFM image with a size of $5 \times 5 \mu\text{m}^2$. For the donor–acceptor mixture, the correlation length also grows from 50 to 58 nm, but the roughness increase from 0.4 to 0.6 nm is especially noticeable (see Fig. 4). Such behavior is likely related to the enhancement of phase separation during annealing and to the formation of domains that are more compact in each of the phases.

The structure of the samples was studied by GIWAXS. The diffraction pattern from a thin PTQ/PNDIT film obtained from toluene exhibits an intense meridian peak that corresponds to the formation of a lamellar phase in donor and acceptor domains with layers that are parallel to the substrate

and have approximately the same interplanar spacing of 24 Å (Fig. 5a). In the range of large angles at the equator, two narrow peaks are observed at 4.1 and 4.3 Å. These peaks indicate the formation of π - π stacking in the direction parallel to the film surface in donor and acceptor domains. Annealing the sample at 100°C reduces the interplanar distance to 21 Å and improves the layer orientation (Fig. 5c). The π - π stacking peak at 4.1 Å disappears; this is related to the destruction of the regular structure in PNDIT domains, as was shown before [19]. It was established that the structure of a film produced from chlorobenzene is noticeably different from that of the above-described film produced from toluene (Fig. 5b). The layer orientation is much weaker, although the interplanar distance reduces to 22.4 Å. In addition, the diffraction pattern does not exhibit a π - π stacking peak; this indicates low ordering within a layer. Annealing decreases the interplanar distance to 20.6 Å and also increases the intensity of the main peak (Fig. 5d). It is interesting to note that the intensity of the amorphous

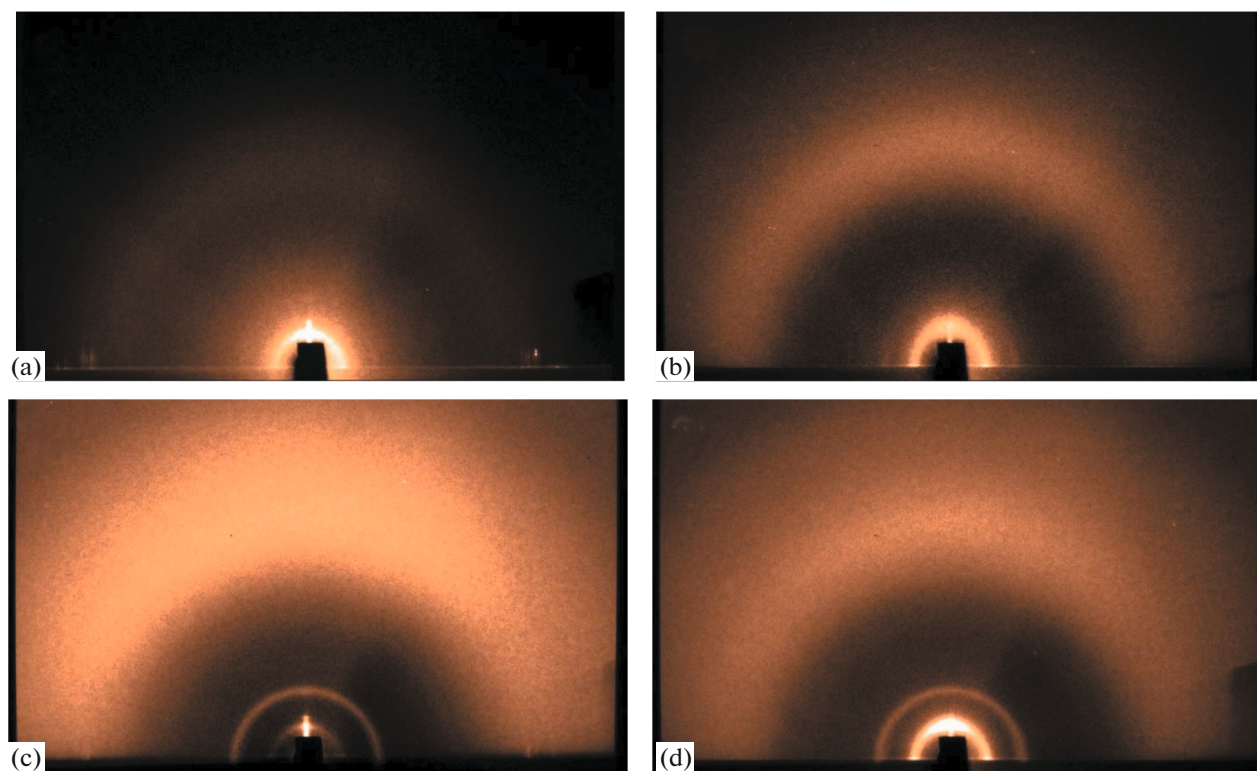


Fig. 5. (Color online) Two-dimensional GIWAXS diffraction patterns from PTQ/PNDIT films prepared from the solution of (a, c) toluene and (b, d) chlorobenzene (a, b) prior to and (c, d) after annealing at 100°C.

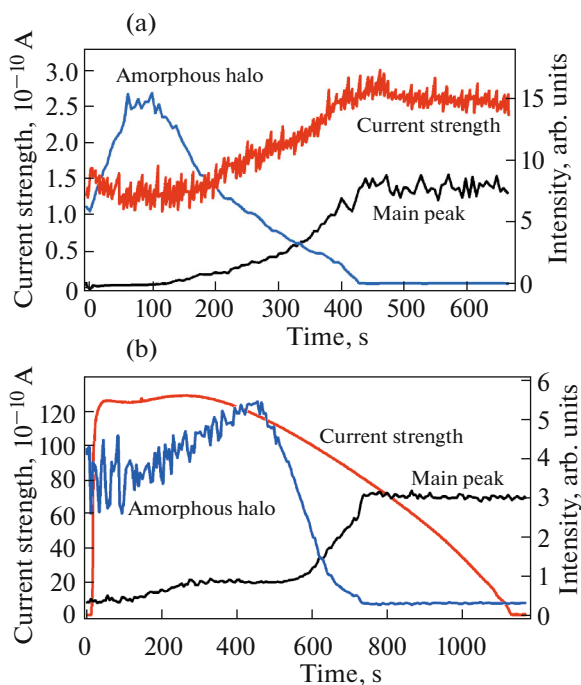


Fig. 6. (Color online) Time dependence of the current strength (red curve) and the intensities of the amorphous-halo (blue curve) and main layered-phase (black curve) peaks in PTQ/PNDIT2 films prepared from (a) toluene and (b) chlorobenzene.

halo of the films produced from chlorobenzene is noticeably higher than that of the films produced from toluene. This may be related to the fact that the solvent has not been completely removed from the film during drying and prevents the formation of ordered domains.

The peculiarities of structure shaping were studied in an experiment on the formation of a film in which both the structure and current strength were measured concurrently (Fig. 6).

The solvent evaporation rate can be estimated by measuring the intensity of the amorphous halo that is typical of scattering on the solvent. For a toluene film, the halo intensity at first grows, which can probably be explained by a reduction in the beam absorption coefficient by a drying droplet (Fig. 6a). The intensity then decreases in two stages due to the solvent being removed from the polymer bulk. The first stage (up to 250 s) is characterized by a sharp decrease in the intensity, while at the second stage (from 250 to 500 s) the intensity reduces gradually. The presence of the two stages is also observed for the current passing through the film. We observed a similar two-stage process before when forming films from P3HT/PCBM and P3HT/ICBA mixtures and explained it by specific features of donor phase separation [14]. Unlike for systems with PCBM, no dramatic intensity increase of the main peak at 24 Å occurs for a polymeric mixture; this indicates that layered structure is formed gradually.

The picture looks noticeably different for a chlorbenzene film (Fig. 6b). The intensity of the amorphous halo gradually increases for the first 550 s, which is related to a slower solvent evaporation rate and its higher absorptivity. Then the intensity sharply decreases; this indicates the formation of a compact film. The intensity of the main peak of the layered structure also changes only slightly during the slow process of chlorbenzene evaporation, but then a dramatic growth is observed that is associated with the formation of regular layers. Therefore, two clear stages can be distinguished in the formation of a film from the donor–acceptor mixture viz. slow evaporation of solvent and rapid compaction of layers. Most likely, this is due to the short duration of the second stage, so the order inside a layer does not have enough time to form, with the lack of a π - π stacking peak indicating the same. The dependence of the current strength is of a descending nature; this indicates that chlorbenzene, which has a conductivity four orders of magnitude higher than that of toluene, is the main current conductor in the system [20]. In the future, we plan to revamp the measurement cell to exclude the effect of conductivity of solvents and widen their variety.

CONCLUSIONS

The influence of the solvent and preparation conditions on the structure of active layers in polymer–polymer solar panels has been demonstrated in this work. AFM and grazing-incidence wide-angle X-ray scattering were used to establish that annealing films improves phase separation and furthers the formation of domains that are more compact. Real-time measurements of the formation of films from nonpolar (toluene) and polar (chlorbenzene) solvents were also taken. It was discovered that toluene film is formed in two stages; this can be ascribed to the phase separation of the donor and acceptor and compaction of layers in the domains. The intensity of the main peak of the lamellar structure increases monotonically in the course of film formation. The formation of chlorbenzene film also occurs in two stages. At the first stage, when the solvent is slowly evaporated, film formation is only weakly expressed. Then, at the second stage, layer compaction starts and is accompanied by a sharp increase in the intensity of the main peak of the layered phase. The results demonstrate the importance of using real-time structural analysis combined with the measurements of physical properties and help understanding the processes that govern the morphology of active layers in organic solar cells.

ACKNOWLEDGMENTS

The authors express their gratitude to D. Portale and V. Bras for technical assistance in X-ray diffraction experiments on the BM26 line at the European Synchrotron Radiation Facility (Grenoble, France). This work was supported by the Ministry of Education and Science of the Russian Federation, project

no. 14.604.21.0121 (RFMEFI60414X0121). AFM measurements were taken with equipment provided by the resource center of scanning probe and electron microscopy at the National Research Center “Kurchatov Institute.”

REFERENCES

1. Z. He, C. Zhong, S. Su, M. Xu, H. Wu, and Y. Cao, *Nat. Photon.* **6**, 591 (2012).
2. H.-Y. Chen, J. Hou, S. Zhang, Y. Liang, G. Yang, Y. Yang, L. Yu, Y. Wul, and G. Li, *Nat. Photon.* **3**, 297 (2009).
3. J. Peet, J. Y. Kim, N. E. Coates, W. L. Ma, D. Moses, A. J. Heeger, and G. C. Bazan, *Nat. Mater.* **6**, 497 (2007).
4. C. R. McNeill and N. C. Greenham, “Conjugated polymer blends for optoelectronics,” *Adv. Mater.* **21**, 3840 (2011).
5. E. J. Zhou, J. Z. Cong, Q. Z. Wei, K. Tajima, C. H. Yang, and K. Hashimoto, *Angew. Chem. Int. Ed.* **50**, 2799 (2011).
6. D. Mori, H. Benten, J. Kosaka, H. Ohkita, S. Ito, and K. Miyake, *ACS Appl. Mater. Inter.* **3**, 2924 (2011).
7. D. Mori, H. Benten, H. Ohkita, S. Ito, and K. Miyake, *ACS Appl. Mater. Inter.* **4**, 3325 (2012).
8. N. Zhou, H. Lin, S. J. Lou, X. Yu, P. Guo, E. F. Manley, S. Loser, P. Hartnett, H. Huang, M. R. Wasielewski, L. X. Chen, R. P. H. Chang, A. Facchetti, and T. J. Marks, *Adv. Energ. Mater.* **4** (3), 1300785 (2014).
9. Y. He, Z. Chen, Y. Zheng, C. Newman, J. R. Quinn, F. Dötz, M. Kastler, and A. Facchetti, *Nature* **457**, 679 (2009).
10. J. C. Blackesley, M. Schubert, R. Steyrlleuthner, Z. H. Chen, A. Facchetti, and D. Neher, *Appl. Phys. Lett.* **99**, 183310 (2011).
11. R. Steyrlleuthner, M. Schubert, F. Jaiser, J. C. Blackesley, Z. H. Chen, A. Facchetti, and D. Neher, *Adv. Mater.* **22**, 2799 (2010).
12. R. Steyrlleuthner, M. Schubert, I. Howard, B. Klaumünzer, K. Schilling, Z. Chen, P. Saalfrank, F. Laquai, A. Facchetti, and D. Neher, *J. Am. Chem. Soc.* **134**, 18303 (2012).
13. M. Al-Ibrahim, O. Ambacher, S. Sensfuß, and G. Gobsch, *Appl. Phys. Lett.* **86** (20), 201120 (2005).
14. K. Kvamen, S. Grigoryan, D. V. Anokhin, V. A. Bataev, A. I. Smirnov, and D. A. Ivanov, *Nanotechnol. Russ.* **10**, 600 (2015).
15. E. Mikayelyan, A. V. Bakirov, M. A. Shcherbina, S. N. Chvalun, S. A. Ponomarenko, and S. Grigorian, *RSC Adv.* **5**, 1319 (2015).
16. L. Grodd, U. Pietsch, and S. Grigorian, *Macromol. Rapid Commun.* **33**, 1765 (2012).
17. E. Ahmed, G. Q. Ren, F. S. Kim, E. C. Hollenbeck, and S. A. Jenekhe, *Chem. Mater.* **23**, 4563 (2011).
18. D. R. Strel'tsov, A. I. Buzin, E. I. Grigor'ev, P. V. Dmitriyakov, K. A. Mailyan, A. V. Pebalk, and S. N. Chvalun, *Nanotechnol. Russ.* **3**, 494 (2008).
19. D. V. Anokhin, K. L. Gerasimov, A. Kiriy, and D. A. Ivanov, *Appl. Mech. Mater.* **792**, 640 (2015).
20. *Physical Encyclopedia*, Ed. by A. M. Prokhorov (Sovetskaya Entsiklopediya, Moscow, 1988) [in Russian].

Translated by V. Potapchouck